Journal of Power Sources 265 (2014) 67–74

Contents lists available at ScienceDirect

Journal of Power Sources

journal homepage: www.elsevier.com/locate/jpowsour

Effect of surfactants on the electrochemical behavior of $LiFePO_4$ cathode material for lithium ion batteries

K. Bazzi [a], B.P. Mandal [a], M. Nazri [a], V.M. Naik [b], V.K. Garg [c], A.C. Oliveira [c], P.P. Vaishnava [d], G.A. Nazri [a,*], R. Naik [a,*]

[a] Department of Physics and Astronomy, Wayne State University, Detroit, MI 48201, USA
[b] Department of Natural Sciences, University of Michigan–Dearborn, Dearborn, MI 48128, USA
[c] Universidade de Brasilia, Instituto de Fisica, 70919-970 Brasilia, DF, Brazil
[d] Department of Physics, Kettering University, Flint, MI 48504, USA

HIGHLIGHTS

- A news process is developed for preparation of conductive carbon coated $LiFePO_4$.
- Nature of carbon-coating plays a critical role in the electrochemical performance.
- Mössbauer spectroscopy identifies the presence of amorphous impurity phases.
- Lower concentration of impurity phases led to a better electrochemical performance.
- $LiFePO_4$ made in presence of lauric acid may be a promising material for lithium secondary batteries.

ARTICLE INFO

Article history:
Received 4 March 2014
Received in revised form
14 April 2014
Accepted 15 April 2014
Available online 26 April 2014

Keywords:
Lithium battery
Surfactant
Mossbauer
Nanomaterials

ABSTRACT

The application of lithium iron phosphate as positive electrode material for lithium ion batteries has been challenged by its poor electronic conductivity. To improve its conductivity and electrochemical performance, we have synthesized $LiFePO_4$/C composite cathode materials by sol gel technique using long chain fatty acids, such as, lauric, myristic, and oleic acids, as surfactants for carbon coating. The phase purity of the three $LiFePO_4$/C composites was confirmed by X-ray diffraction. The Raman spectroscopy, scanning electron microscopy and transmission electron microscopy measurements show that the surfactants coat the $LiFePO_4$ particles with carbon with varying degree of uniformity depending on the surfactant used. The sample prepared in presence of lauric acid shows smaller particle size and the lowest charge transfer resistance, higher Li-ion diffusion coefficient, higher discharge capacity ($\sim$155 mAh g^{-1} at C/3 rate), better rate capability and cyclic stability compared to the other two samples. We found the smaller particle size, uniformity of carbon coating, reduced agglomeration, and a lower amount of Fe^{3+} impurity phase in the samples to be major contributing factors for better electrochemical properties in the $LiFePO_4$/C cathode material.

© 2014 Elsevier B.V. All rights reserved.

1. Introduction

Lithium iron phosphate ($LiFePO_4$) has been intensely investigated since it was proposed by Padhi et al. [1] as a possible cathode material for Li-ion rechargeable batteries. The olivine structured $LiFePO_4$ has a remarkable thermal stability, a relatively high theoretical specific capacity of 170 mAh g^{-1} and a flat charge–discharge profile at $\sim$3.4 V vs. Li^+/Li [1,2]. In addition, it is inexpensive and environment friendly compared to cobalt-oxide-based materials, particularly, for large-scale applications such as hybrid electric vehicles (HEV) and plug in electric vehicles.

Despite the highly desirable properties of $LiFePO_4$ as a cathode material, it has been difficult to utilize its full potential due to its intrinsic poor electronic conductivity which leads to high impedance, low capacity, poor rate capability, and low diffusion rate of Li^+ ion across the $LiFePO_4$/$FePO_4$ boundary [3]. Large-size Li-ion batteries in electrical vehicles and hybrid electric vehicles require high power density (high rate), high energy density (extended range), and must meet the strict safety regulations. In order to meet the requirements of these energy storage devices, considerable efforts

* Corresponding authors.
E-mail addresses: nazri@wayne.edu (G.A. Nazri), rnaik@wayne.edu (R. Naik).

http://dx.doi.org/10.1016/j.jpowsour.2014.04.069
0378-7753/© 2014 Elsevier B.V. All rights reserved.

have been made to increase the conductivity of $LiFePO_4$ by decreasing its particle size down to nanometers [4–7], and coating with electronic conducting agents [8–12]. It has also been shown that doping $LiFePO_4$ with supervalent ions improves its electrical conductivity [13–16].

Carbon coating is one of the most commonly used methods for enhancing the electrical conductivity and the electrochemical performance of $LiFePO_4$. The major role of the carbon coating is not only to significantly increase the electrical conductivity, but also to control the particle size by inhibiting the particle growth. The smaller particle size would be favorable for shortening the diffusion length of lithium ions. It has been found that the electrochemical properties of $LiFePO_4$ are strongly influenced by the quality of the carbon coating, amount of carbon, the degree of graphitization, morphology and the distribution of the carbon on the $LiFePO_4$ surface and in the grain boundaries [17,18]. The degree of graphitization of the carbon, which is mainly determined by the carbon source used, is one of the important factors for the conductivity and rate behavior of $LiFePO_4$ [19,20]. The sp^2 carbon coating is much more effective than sp^3 carbon for improving electrical conductivity [21], and $LiFePO_4$ coated with more graphitic carbon shows higher conductivity and exhibits better electrochemical properties [22]. The ratio of carbon in disordered/graphitic (D/G) is often determined by the intensities of the Raman bands associated with sp^2/sp^3 vibrations [21].

Many carbon sources such as sucrose [23], carbonaceous polymers [24], aromatic diketones [25], carbon rich precursors [26], have been used in the past to coat $LiFePO_4$ particles. Different methods for carbon coating, such as adding vapor grown carbon fibers [27], carbon nanotubes [28] and graphene sheets [29] have been used and the results indicate that the carbon precursors have a strong influence on the properties of the $LiFePO_4$/C composites [30]. It has been shown that the amount of carbon has a profound influence on the specific capacity of $LiFePO_4$ and is found to increase with increasing carbon content up ~12% and a further increase in carbon leads to a rapid decrease in specific capacity [31,32]. Several explanations have been proposed for the poor performance, such as, the amorphous carbon diluting the density of the crystallite $LiFePO_4$, the excess carbon suppressing the formation of crystalline $LiFePO_4$, and the formation of Fe_2P phase due to reduction of Fe and P because of high carbon content and the high temperature used for preparing the samples. It is therefore very important to have the correct amount of carbon for optimizing the electrochemical properties and performance of $LiFePO_4$ cathode material.

Further, the thickness of carbon coating has been shown to play an important role in determining the conductivity of $LiFePO_4$. A thickness of 3–8 nm seems to be optimum in producing the best discharge capacity due to the easy diffusion of lithium ion [33,34]. A number of organic precursors have been used for carbon coating, including, sucrose, glucose, organic carboxylic acid, citric acid and other organic reagents due to their low calcinations temperatures [35–37].

In any chemical reaction, surface of the material plays an important role. The surface properties of $LiFePO_4$ are unknown, whether it is polar or non polar, hydrophobic or hydrophilic, depend on the synthesis technique and the nature of the material used for coating. An organic material with multiple functional groups, such as surfactants, can favorably interact with the complex surface structure of $LiFePO_4$ very well because the surfactants are surface active compounds that are amphiphiles which consist of a polar ionic or non-ionic head and hydrophilic tail. Most surfactants are carbon rich materials, such C_{12} and C_{14} fatty acids, and in some studies olive oil, soybean oil and butter have been used for carbon coating $LiFePO_4$ [38]. Fatty acids can coat $LiFePO_4$ in different ways, including micelle or reverse micelles or their long chains can wrap around the active material. It is of interest to study the effects of coating with saturated and unsaturated fatty acid and determine the effects on uniformity of carbon coverage, particle size, morphology, and rate capability of the cathode material.

The other factor that influences the properties and performance of $LiFePO_4$ as a cathode material is the presence of the impurity phases. Impurity phases, with higher conductivity, that precipitate at the grain boundaries have been shown to improve rate capability [39–41]. However, the effect of impurities on electronic conductivity and electrochemical performance is poorly understood as some impurities favorably impact electronic conductivity and electrochemical performance whereas others affect adversely. It is generally observed that most impurities that appear as Fe (III) ion prevent $LiFePO_4$ from achieving its optimum performance.

In this study, we have investigated $LiFePO_4$/C composite materials prepared by sol–gel technique using lauric, myristic and oleic acids as surfactants for carbon coating. Lauric acid ($C_{12}H_{24}O_2$) and myristic acid ($C_{14}H_{28}O_2$) are saturated fatty acids with no –C=C– double bonds whereas the oleic acid ($C_{18}H_{34}O_2$) is a monounsaturated fatty acid containing one double bond. These fatty acids, which differ in chain length and chemical bonds, may assist the formation of nano-sized $LiFePO_4$ particles, influence the nature of carbon being deposited on these particles affecting the electronic conductivity, and hence the electrochemical properties of $LiFePO_4$/C composites. The structural and physical properties of $LiFePO_4$/C composites were characterized by X-ray diffraction (XRD), transmission electron microscopy (TEM) and scanning electron microscopy (SEM), and Raman Spectroscopy. ^{57}Fe Mössbauer spectroscopy has been used to identify the Fe (III) impurity phases. The electrochemical properties (charge transfer resistance, Li-ion diffusion coefficient, charge/discharge capacity, rate capability and cyclic stability) have been measured and correlated with their particle size and morphology. We find the particle size, morphology, quality of the carbon coating, and the impurity phases significantly influence the electrochemical behavior of the cathode materials.

2. Experimental detail

2.1. Synthesis procedure

$LiFePO_4$ and carbon coated $LiFePO_4$/C samples were prepared by sol–gel technique, by mixing $CH_3CO_2Li \cdot 2H_2O$ (lithium acetate dihydrate, 99%, Alfa Aesar), $FeCl_2 \cdot 4H_2O$ (ferrous chloride, Fisher Scientific), and P_2O_5 (phosphorous pentoxide, Fisher Scientific) as precursors in stoichiometric ratio. We separately dissolved 1.990 g of ferrous chloride and 0.708 g of phosphorous pentoxide each in 10 ml of ethanol (200 proof). These solutions were mixed together under nitrogen environment and stirred for 3 h for homogeneous mixing. We also dissolved 1.019 g of lithium acetate in 10 ml of ethanol. The lithium acetate solution was added to the previous mixed solution of ferrous chloride and phosphorous pentoxide and stirred under nitrogen environment for another 3 h to allow the sol formation. For preparing the carbon coated samples, we dissolved separately 1.500 g of lauric acid, 1.710 g of myristic acid, and 2.115 g of oleic acid (LA, MA or OA), each in 10 ml of dry ethanol. The selected surfactant was then added to the above final mixture and stirred for another 3 h under nitrogen environment. The resultant sol was then dried at 80 °C to form dry powder which was then ground and annealed under reduced environment of H_2 (10%) and Ar (90%) at 600 °C for 5 h. Carbon content of the samples was measured by CHN elemental analyzer, where, the sample is combusted in a pure oxygen environment; the gases are carried through the system by helium, converted and measured as CO_2, H_2O and N_2. The product gases are separated under steady-state conditions and are detected by thermal conductivity. The overall

carbon content was found to be approximately 8% in these three samples. In what follows, we refer to the samples prepared with lauric, myristic and oleic acids as sample A, B, and C, respectively, and the bare $LiFePO_4$ without any additive as sample D.

2.2. Characterization

XRD patterns of the samples were recorded using a Rigaku Miniflex 600 powder diffractometer. Raman spectra of the samples were measured using a Jobin–Yvon Horiba Triax 550 spectrometer, a liquid-nitrogen cooled charge-coupled device (CCD) detector, an Olympus model BX41 microscope with a 100× objective, and a Modu-Laser (Stellar-Pro-L) Argon-ion laser operating at 514.5 nm. The laser power at the sample was maintained at very low level (~1 mW) to avoid any sample heating effects. Each spectrum was averaged over three accumulations with 10 s integration time. The resolution of the spectrometer using 1200 grooves mm^{-1} grating was ~3.5 cm^{-1}. The morphology of the bare and $LiFePO_4$/C powders was investigated using a JSM-6510-LV-LGS SEM and JEOL 2010 TEM instruments.

^{57}Fe Mössbauer spectra were recorded in the transmission geometry using both sides of a (Wissel) transducer coupled to ^{57}Co in Rh matrix source of about 50 mCi and 256 channels of a multichannel analyzer. The velocity calibration and the linearity verification were performed using a thin iron foil. For Mössbauer measurements, approximately 70 mg of the sample was uniformly dispersed in a Teflon circular cell of 1.7 cm diameter. The isomer shift values are reported with reference to α-Fe foil. The spectra were least square fitted with MossWin program.

The electrochemical properties were measured using a standard CR2032 coin cell geometry with lithium metal as an active anode. The fabrication details of the electrochemical cell are described elsewhere [42]. In brief, the active materials and Super P carbon, as a conducting material, were mixed in 80:20 ratio and ground for 20 min. The homogenous mixture was then put on an aluminum mesh and pressed between two steel cylinders. The aluminum mesh acts as a current collector and provides good adhesion to the mixture of active material. It is advantageous to test intrinsic property of active electrode materials without the contribution from the binders. There have been many fundamental studies on cathode materials without the use of binders, such as single particle electrochemistry [43], solid-state pellets for in-situ work [44,45], and thin films produced by sputtering [46]. One advantage of testing cathode materials without the binder is that the effects and contributions of the binder on electrochemical properties of the materials are eliminated [29].

The cathode was charged and discharged against Li metal electrode that served as a counter electrode separated by Celgard 2400 polymeric separator soaked with binary electrolyte consisting of ethylene carbonate and dimethyl carbonate, (50:50) containing 1 M $LiPF_6$ in the coin cell geometry. Electrochemical impedance measurements were carried out using a Gamry electrochemical measurement system (EIS 300) in the frequency range of 0.1–100 kHz with an AC amplitude of 10 mV. The room temperature cyclic voltammetry (CV) measurements were carried out using a Gamry electrochemical system (PHE 200) in the range of 2.6–4.2 V at different scan rates. The galvanostatic charge and discharge measurements were performed with different currents in the voltage range of 2.2–4.2 V.

3. Results and discussion

3.1. X-ray diffraction

The XRD patterns (Fig. 1) confirm the phase purity of crystalline $LiFePO_4$/C samples (A–C), and bare $LiFePO_4$ sample (D). Clearly, XRD patterns look similar and the Bragg peaks can be indexed to a single and well crystallized $LiFePO_4$ phase possessing an ordered olivine structure with a *Pnma* space group (PDF file No: 40-1499). This indicates that the addition of carbon using surfactants has no negative influence on the formation of $LiFePO_4$ crystal structure in these samples. The crystallite size d was calculated using the Scherrer's equation: $d = \kappa\lambda/(\beta \cos\theta)$, where β is the corrected full-width at half-maximum of the diffraction peak on the 2θ scale and κ is chosen as a constant (0.9) for all samples. The crystallite sizes for sample A, B, C, and D were found to be approximately 28, 30, 40 and 50 nm, respectively. Thus, the mean crystallite size of the $LiFePO_4$ decreased when the fatty acids are used to in the synthesis $LiFePO_4$/C composite nanostructures.

3.2. Scanning electron microscopy

Fig. 2(a)–(d) shows the SEM images of samples A, B, C and D. The carbon coated samples show distinctly different morphology and microstructure compared to the bare $LiFePO_4$ sample. The carbon coated samples, particularly, for samples A and B prepared with lauric and myristic acids show fine grains (~0.1 μm) with uniform morphology and porosity compared to sample C prepared with oleic acid and sample D (without surfactant). Perhaps the smaller grains allow shorter diffusion length for Li ions in the intercalation/deintercalation process, and thus the type of fatty acid used to prepare $LiFePO_4$/C plays a crucial role in controlling the morphology, the grain size, and hence electrochemical properties.

3.3. Transmission electron microscopy

To investigate the nature of the carbon coverage in the $LiFePO_4$/C samples, TEM measurements were performed and the results are shown in Fig. 3(a)–(d) for samples A, B, C and D. The wiring effect of carbon in connecting interfaces between $LiFePO_4$ particles leading to a remarkably enhancement in electrical conductivity, especially with uniform carbon coating, has been reported [39,47]. Samples A–C clearly show the presence of carbon coverage around $LiFePO_4$ particles with differing uniformity. The sample A, prepared with lauric acid, shows 30–50 nm sized particles coated with carbon of ~8 nm thickness. On the other hand, samples B and C, prepared with myristic and oleic acids, show slightly larger size particles (50–100 nm) with regions of carbon interspersed between them.

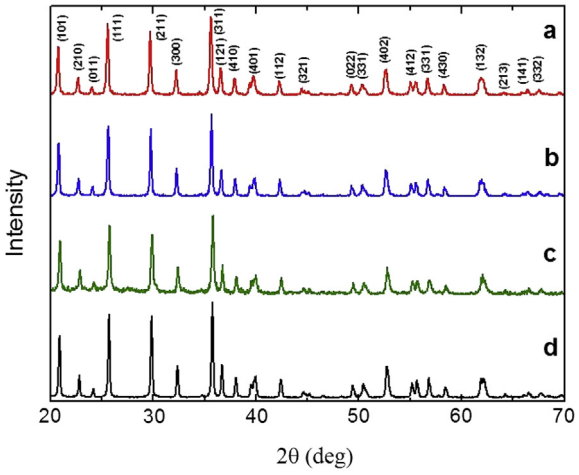

Fig. 1. XRD patterns of $LiFePO_4$/C and $LiFePO_4$ samples $LiFePO_4$/LA (a), $LiFePO_4$/MA (b), $LiFePO_4$/OA (c) and $LiFePO_4$ (d).

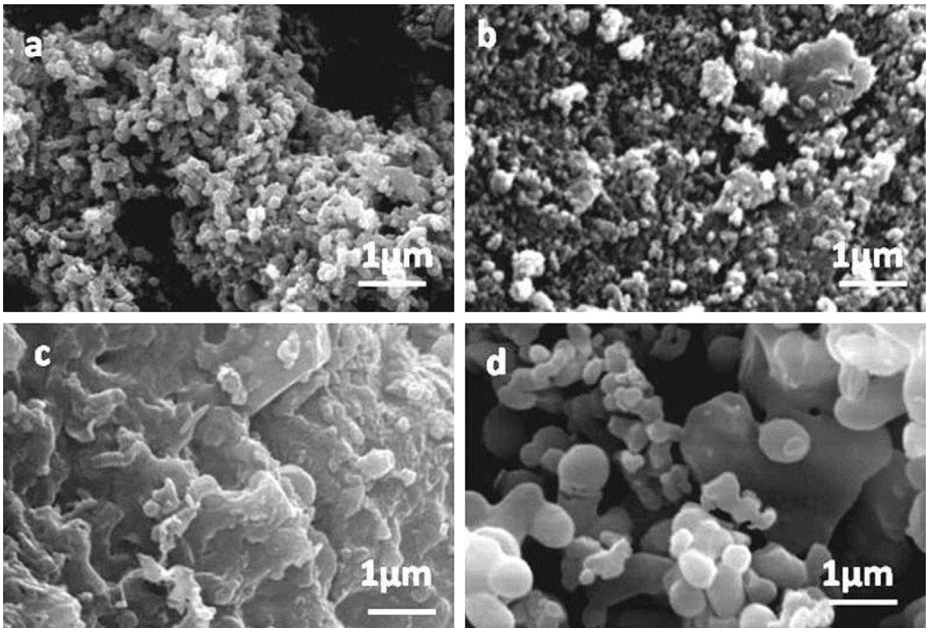

Fig. 2. SEM images of $LiFePO_4$/C and $LiFePO_4$ samples $LiFePO_4$/LA (a), $LiFePO_4$/MA (b), $LiFePO_4$/OA (c) and $LiFePO_4$ (d).

3.4. Raman spectroscopy

Raman spectroscopy is a very useful tool for investigating the nature of carbon in $LiFePO_4$/C samples. Fig. 4(a)–(d) shows the Raman spectra of carbon-coated and the bare $LiFePO_4$ samples. $LiFePO_4$ (Fig. 4(d)) shows the expected internal, bands arising from the intra-molecular vibrations of the PO_4^{3-} anion that occur above 800 cm^{-1}, and the external modes (lattice vibrations), that occur below 800 cm^{-1} which arise primarily due to the vibrational motions related to FeO_6 and LiO_6 octahedra [41,48]. The $LiFePO_4$/C samples show two strong and broad bands centered ~1340 and 1594 cm^{-1} which are commonly observed in disordered carbons and are labeled as D and G bands [48]. The bands due to $LiFePO_4$ particles are not seen in these spectra as the incident laser power was kept low (1 < mW) to prevent the decomposition of the sample due to laser beam heating, especially in the presence of carbon layer.

The band at ~1600 cm^{-1}, whose position is close to that of the E_{2g} mode of crystalline graphite, is assigned to the so-called G band, and the broad-band at 1340 cm^{-1}, so called the D band is associated with disorder induced mode of graphite near the zone-edge K point [49–51]. As the Raman bands in D and G region of the spectra are broad

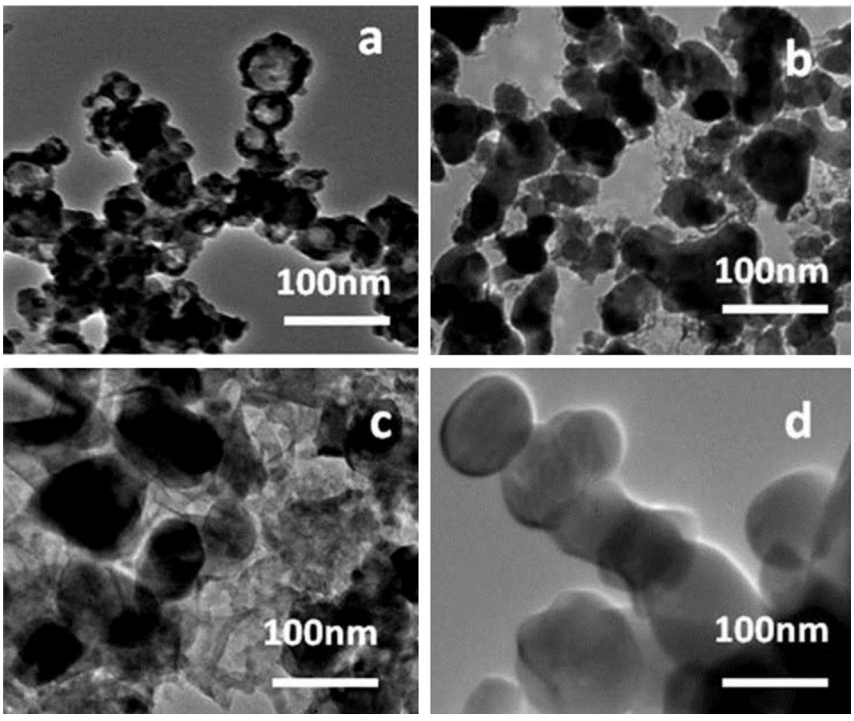

Fig. 3. TEM images of $LiFePO_4$/C and $LiFePO_4$ samples $LiFePO_4$/LA (a), $LiFePO_4$/MA (b), $LiFePO_4$/OA (c) and $LiFePO_4$ (d).

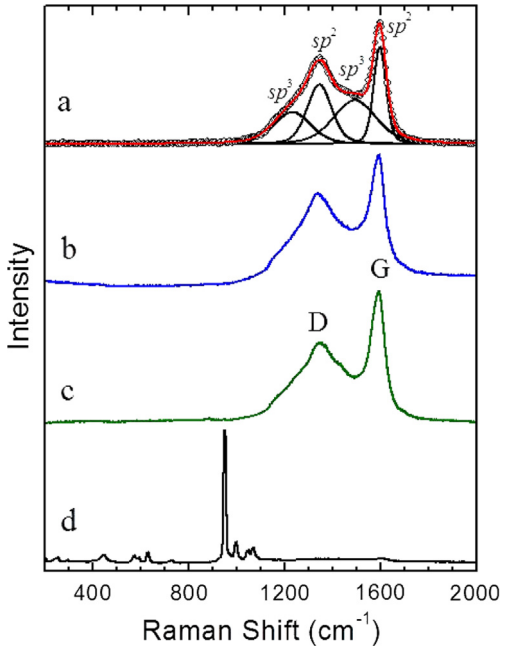

Fig. 4. Raman spectra of $LiFePO_4$/C and $LiFePO_4$ samples $LiFePO_4$/LA (a), $LiFePO_4$/MA (b), $LiFePO_4$/OA (c) and $LiFePO_4$ (d). Deconvolution of D and G bands is also shown for sample $LiFePO_4$/LA in (a).

the intensity profiles are often deconvoluted using four Gaussians or Gaussian–Lorentzian lines [46] and the two additional bands needed to satisfactorily fit the intensity profiles occur ~1205 and 1520 cm^{-1} and are assigned to sp^3 type carbon which are often observed in amorphous carbonaceous compounds. The intensity ratios of the D and G bands (I_D/I_G) or the total intensity associated with sp^2 to sp^3 type carbon vibrations is often used to evaluate the nature of the carbon using the deconvoluted Raman bands [17]. We have fitted the Raman intensity profiles using four Gaussian–Lorentzian lines (for example see Fig. 4(a)) and have estimated the intensity ratios I_D/I_G and $I_{sp2}/I_{sp3} = (I_{1340} + I_{1595})/(I_{1205} + I_{1520})$. For all the three samples, A, B, and C, we found very similar values for $I_D/I_G \sim 2$ and $I_{sp2}/I_{sp3} \sim 1.2$, which clearly indicate that the nature of the carbon is very similar in three $LiFePO_4$/C samples.

3.5. ^{57}Fe Mossbauer spectroscopy

The room temperature ^{57}Fe Mössbauer spectra for carbon coated samples A–C are shown in Fig. 5(a)–(c). All the samples show a dominant symmetric doublet with an isomer shift (IS) ~1.22 mm s^{-1} and a quadruple splitting (QS) of ~2.94 mm s^{-1}, in agreement with the literature values for Fe^{2+} high spin configuration of the 3*d* electrons and the distorted environment at the Fe atom in $LiFePO_4$ [52–54]. In addition, we notice another doublet with IS ~0.42 mm s^{-1} and a QS ~0.82 mm s^{-1} which is assigned to ferric iron in the sample originating mostly from amorphous impurity phases such as $FePO_4$ and/or Fe_2P produced by high temperature annealing in a partial reducing environment of Ar/H_2 atmosphere. As lithium compounds have higher vapor pressure at elevated temperatures, the lithium deficiency in the final compound ($LiFePO_4$) may result, even though stoichiometric amounts of precursors are used in the initial synthesis process. Compared to $LiFePO_4$, the value of IS for this impurity doublet is smaller because the removal of lithium is accompanied by a decrease of one of Fe 3*d* electron per Fe changing from high spin Fe^{2+} (in $LiFePO_4$) to high spin Fe^{3+} (in $FePO_4$). The larger width of the peak clearly indicates the amorphous nature of this phase.

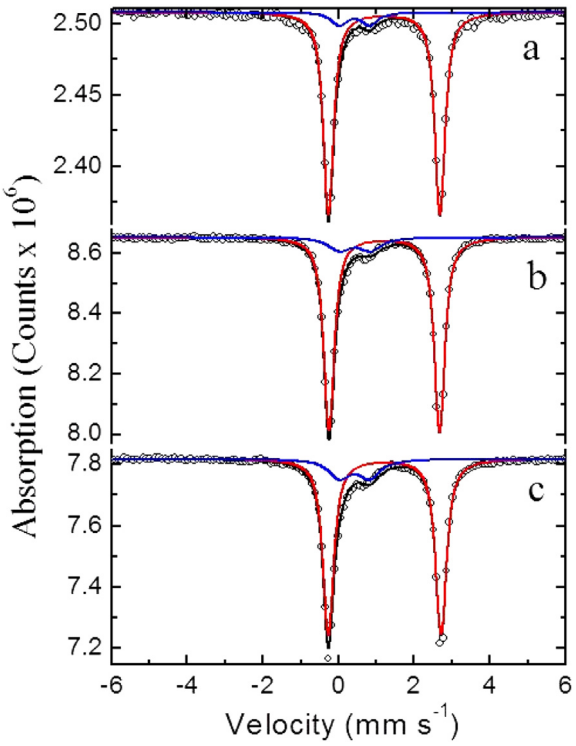

Fig. 5. Mössbauer spectra of $LiFePO_4$/C samples $LiFePO_4$/LA (a), $LiFePO_4$/MA (b) and $LiFePO_4$/OA (c).

The values of the Mössbauer parameters and the composition of the phases for carbon-coated samples are listed in Table 1. It is interesting to note that the amount of the Fe^{3+} impurity phase increases from 9% in sample A (prepared with lauric acid) to 17% in the sample C (prepared with oleic acid). As discussed later, the samples with smaller amount of impurity phase show larger capacity and improved electrochemical properties.

3.6. Electrochemical measurements

Fig. 6 shows the Nyquist plots for samples A, B, C and D. The curves consist of two distinct parts: a semicircle and an inclined line. Based on a simple equivalent circuit model the first intercept of the semicircle on the real part of the impedance plot represents the electrolyte solution resistance R_s, diameter of the semicircle gives the value of charge transfer resistance R_{ct}, and the inclined line represents Warburg's resistance, R_w, mainly due to ion diffusion. As the charge transfer at the lithium surface (anode) is fast and has a high exchange current density, the impedance plot is dominated by the charge transfer at the cathode side. The R_{ct} values are 150, 285, 340, and 585 Ω for samples A, B, C, and D, respectively. Clearly, these

Table 1
^{57}Fe Mossbauer parameters for $LiFePO_4$/C composites synthesized with long chain fatty acids for carbon coating.

Sample	IS (mm s^{-1})	QS (mm s^{-1})	LW (mm s^{-1})	Percentage	Assignment
A ($LiFePO_4$ + LA)	1.22	2.95	0.28	91%	Fe^{2+} ($LiFePO_4$)
	0.42	0.81	0.47	9%	Fe^{3+}
B ($LiFePO_4$ + MA)	1.22	2.92	0.29	87%	Fe^{2+} ($LiFePO_4$)
	0.43	0.82	0.70	13%	Fe^{3+}
C ($LiFePO_4$ + OA)	1.23	2.98	0.31	83%	Fe^{2+} ($LiFePO_4$)
	0.42	0.80	0.66	17%	Fe^{3+}

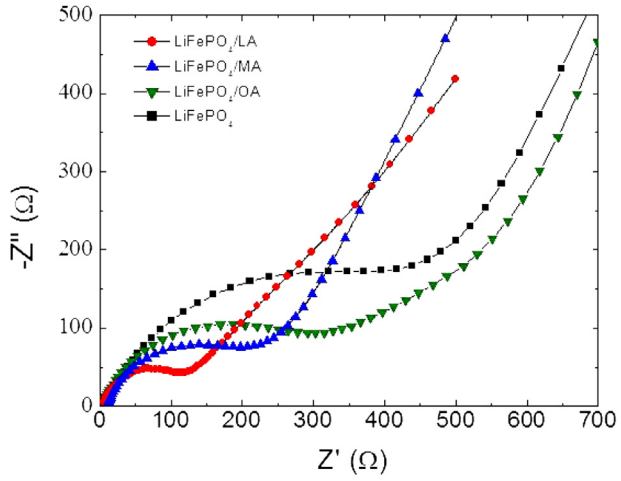

Fig. 6. Nyquist plots of $LiFePO_4$/C and $LiFePO_4$ samples.

results indicate that the conductivity of $LiFePO_4$/C is significantly higher than that of the bare $LiFePO_4$, and the carbon coating leads to a reduction in charge transfer resistance in $LiFePO_4$/C composites. The presence of impurity phases, such as Fe_2P at the grain boundaries, can also influence the electrical conductivity of the particles. Our electrochemical measurements, discussed later, show that the particle size, the degree of agglomeration, and the nature of carbon coating around active electrode material play a key role in enhancing the electrochemical properties of the cathode materials which is in good agreement with previous reports [42,55].

The electrochemical behavior of $LiFePO_4$/C cathodes is characterized by cyclic voltammetry (CV). Fig. 7(a)–(d) shows the CV profiles of $LiFePO_4$/C electrodes at different scan rates in the range of 0.2–5 mV s^{-1}. The CV profiles show anodic (charge) and the cathodic (discharge) peaks corresponding to the charge–discharge reactions of the Fe^{2+}/Fe^{3+} redox couple with midpoint of ~3.43 V, which corresponds to the open-circuit voltage (OCV) of the $LiFePO_4$ electrode [56]. The CV profiles of $LiFePO_4$/C (Fig. 7(a)–(c)) show higher anodic and cathodic peak currents compared to that of bare $LiFePO_4$ (Fig. 7(d)). Furthermore, the peak shapes for the $LiFePO_4$/C samples are sharper compared to the electrode prepared with bare $LiFePO_4$, which has a broad peak indicating a slower kinetics.

From the CV data obtained with a scanning rate of 0.2 mV s^{-1}, the difference between the anodic and cathodic peak voltages (hysteresis) has been found to be ~0.27 V for samples A and B, whereas slightly higher values of 0.31 and 0.40 V for samples C and D. These results are consistent with slower kinetics and larger overpotentials exhibited by samples C and D compared to samples A and B. For small scan rates, the anodic and cathodic peak currents vary nearly linearly with the square root of the scan rate, indicating that the Li-ion insertion/extraction in $LiFePO_4$ is a diffusion controlled process [56]. Fig. 8 shows such plots for anodic currents in samples A–D. In the linear potential sweep voltammogram of a reversible system, the peak current (I_p in amperes) can be expressed using the Randles–Sevčik equation:

$$I_p = 2.69 \times 10^5 \, n^{3/2} C_0^b A D_{Li}^{1/2} \nu^{1/2} \quad (1)$$

where, I_p the peak current value, n is the number of electrons involved in the reaction of the redox couple (for Li^{1+} it is 1), C_0^b is the concentration (0.0228 mol cm^{-3} in our case), A is the effective working electrode area (0.5 cm^2 in our case), ν is the rate at which the potential is swept (V s^{-1}), and D_{Li} is the diffusion coefficient (cm^2 s^{-1}) of Li^+ [57]. According to Eq. (1), I_p versus $\nu^{1/2}$ is linear and the diffusion coefficient can be estimated from the slope of this line, and is estimated to be 2.4×10^{-10}, 0.98×10^{-10}, 0.6×10^{-10}, and 0.9×10^{-11} cm^2 s^{-1} for samples A, B, C, and D, respectively (see Fig. 8). The $LiFePO_4$/C prepared with lauric acid (sample A) exhibits the highest Li-ion diffusion coefficient and the bare $LiFePO_4$ (sample D) the lowest.

Coin cells prepared with $LiFePO_4$ and $LiFePO_4$/C cathodes were galvanostatically charged and discharged between 2 and 4.2 V

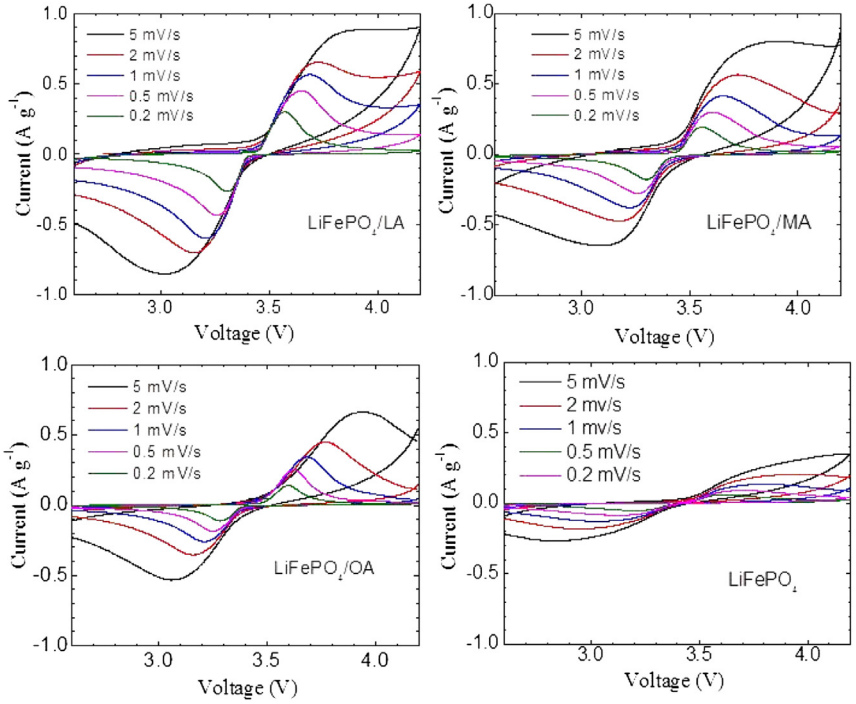

Fig. 7. CV profiles of $LiFePO_4$/C and C–$LiFePO_4$ samples with different scan rates.

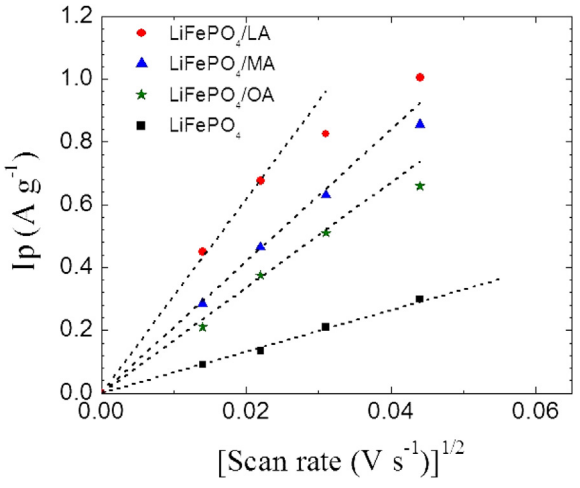

Fig. 8. Randles–Sevčik plot (I_p vs. $\nu^{1/2}$) of normalized peak current vs. square root of the scan rate.

versus lithium at various C-rates. Fig. 9(a) shows the charge–discharge profiles of the cathodes prepared with samples A, B, C, and D measured at a rate of C/3. The flat nature of the charge–discharge potential curves around 3.45 V indicates a typical two phase nature of the lithium extraction and insertion reactions between $LiFePO_4$ and $FePO_4$ [58]. The sloped parts of the profiles at the beginning and at the end refer to the charge transfer activation and concentration polarizations.

The measured specific capacity values at C/3 for samples A, B, C and are 155, 149, 138 and ~65 mAh g^{-1}, respectively, and this observed trend is consistent with the charge transfer resistance of these samples. This clearly shows that the carbon coating of $LiFePO_4$ using surfactants improves the conductivity and hence the specific capacity. The significant improvement observed in the electrochemical kinetics of the $LiFePO_4$/C composite samples could be attributed to a number of factors, such as, improved electrical conductivity, reduced particle size and increased porosity.

The rate capability of the three samples A, B and C was characterized by applying different currents. Fig. 9(b) shows the capacity of samples A, B and C measured at C/2, C/3, 2C and 5C rates during every five cycles. The bare $LiFePO_4$ sample showed very poor performance and therefore is not included here. A gradual decrease in discharge capacity with increase in *C* rate is evident, as is generally the case for all electrodes. This is attributed to the increased IR voltage loss and higher concentration polarization at the electrode/electrolyte interface to meet the fast reaction kinetics at higher *C* rates [59]. At higher C rate (5C), the supply of electrons from the interface electrochemical reaction becomes a problem leading to lower specific capacity. Sample A delivers a specific capacity of 155 mAh g^{-1} (C/3) and shows a similar value during the subsequent 5 cycles (Fig. 9(b)). The discharge capacity decreases while the over-potential increases with increasing C rate. At a higher current density of 5C, the sample A still retains a discharge capacity of ~90 mAh g^{-1}. However, for samples B and C the values drop to 80 and 65 mAh g^{-1}, respectively. Clearly, samples B and C suffer a serious capacity loss at a higher current density of 5C, which may be due to the insufficient surface electronic contact in these samples compared to sample A. As discussed earlier, the grains are completely coated with a uniform carbon layer in sample A and are in close contact with other grains.

Samples A, B and C show excellent cycling stability (see Fig. 9(c)) with specific capacity remaining nearly constant over 100 cycles. However, sample D showed somewhat faster degradation in specific capacity over first few cycles compared to other samples and it

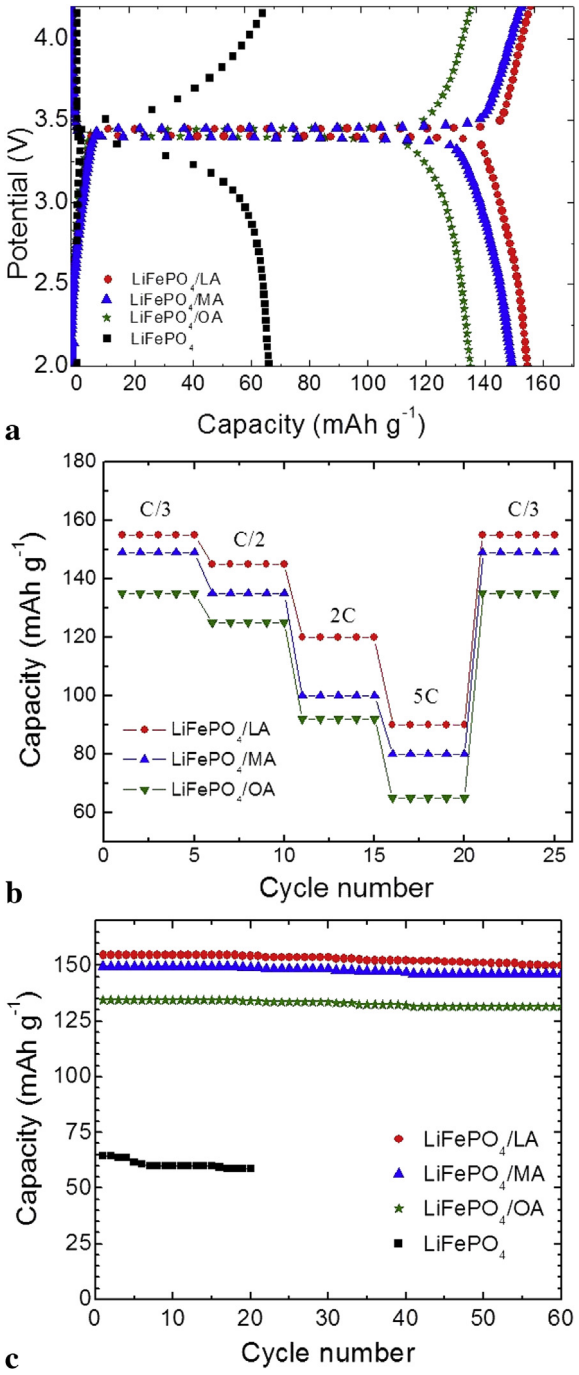

Fig. 9. (a) Galvanostatic charge–discharge cycles for $LiFePO_4$/C and $LiFePO_4$ samples at C/3 rate. (b) Capacity at different rates for $LiFePO_4$/C samples. (c) Capacity vs. cycle number for $LiFePO_4$/C samples at C/3 rate.

failed after 40 cycles. The observed excellent cycling characteristics combined with improved kinetics of $LiFePO_4$ confirm the role of optimizing the particle size, porosity, and electrical conductivity of the $LiFePO_4$ electrode material through effective carbon coating using appropriate surfactant.

4. Conclusions

Nano-sized $LiFePO_4$/C composites with improved electrochemical performance have been synthesized by a sol–gel method

using saturated (lauric and myristic acids) and unsaturated (oleic acid) fatty acids differing in carbon chain length as the sources of carbon. The microstructural investigation of $LiFePO_4$/C samples shows that the particle size and the nature of the carbon coating depend on the type of surfactant used. While all $LiFePO_4$/C samples prepared with three different surfactants show higher specific capacity, improved rate capability, and cycling stability compared to the uncoated $LiFePO_4$ sample, the $LiFePO_4$/C composite prepared with lauric acid exhibits a higher discharge capacity compared to the samples prepared using myristic and oleic acids. Addition of surfactant as a carbon source, has two major advantages 1) it provides superior conductive carbon coating leading to improved electrochemical performance, and 2) it serves as an inhibitor for particle growth, leading to the formation of more uniform sized nanoparticles. Further, our one-pot synthesis process is a versatile method of preparing well controlled and a better quality cathode material. Lauric acid, with a shorter carbon chain length, seems to arrest the particle growth effectively and coat the $LiFePO_4$ particles uniformly with carbon, resulting in lower charge transfer resistance and higher Li-ion diffusion coefficient compared to other two samples. A non-uniform distribution of carbon and a higher amount of ferric impurity phase in $LiFePO_4$/C composites prepared with myristic and oleic acids seem to decrease the charge/discharge capacity. Based on the results, the $LiFePO_4$ coated with lauric acid may be a promising material for lithium secondary batteries.

Acknowledgment

We thank Richard Barber Foundation for financial support for this research.

References

[1] K. Padhi, K.S. Nanjundaswamy, J.B. Goodenough, J. Electrochem. Soc. 144 (1997) 1188.
[2] N. Ravet, Y. Chouinard, J.-F. Magnan, S. Besner, M. Gauthier, M. Armand, J. Power Sources 144 (2001) 1188.
[3] J.M. Tarascon, M. Armand, Nature 414 (2001) 359–367.
[4] S.Y. Lim, C.S. Yoon, J.P. Cho, Chem. Mater. 20 (2008) 4560.
[5] C. Delmas, M. Maccario, L. Croguennec, F. Le Cras, F. Weill, Nat. Mater. 7 (2008) 665–671.
[6] P. Gibot, M. Casas-Cabanas, L. Laffont, S. Levasseur, P. Carlach, S. Hamelet, J.-M. Tarascon, C. Masquelier, Nat. Mater. 7 (2008) 741–747.
[7] F. Hsu, S.-Y. Tsay, B.-J. Hwang, J. Mater. Chem. 14 (2004) 2690–2695.
[8] Y.H. Huang, J.B. Goodenough, Chem. Mater. 20 (2008) 7237.
[9] Z. Chen, J.R. Dahn, J. Electrochem. Soc. 149 (2002) A1184–A1189.
[10] M.M. Doeff, J.D. Wilcox, R. Kostecki, G. Lau, J. Power Sources 163 (2006) 180–184.
[11] R. Dominko, M. Bele, M. Gaberscek, M. Remskar, D. Hanzel, S. Pejovnik, J. Jamnik, J. Electrochem. Soc. 152 (2005) A607–A610.
[12] R. Dominko, M. Bele, J.-M. Goupil, M. Gaberscek, D. Hanzel, I. Arcon, J. Jamnik, Chem. Mater. 19 (2007) 2960–2969.
[13] M. Wagemaker, B.L. Ellis, D.L. Hecht, F.M. Mulder, L.F. Nazar, Chem. Mater. 20 (2009) 6313.
[14] S.Y. Chunga, Y.M. Chiang, Electrochem. Solid-State Lett. 6 (2003) A278–A281.
[15] F. Croce, A. D'Epifanio, J. Hassoun, A. Deptula, T. Olczac, B. Scrosati, Electrochem. Solid-State Lett. 5 (2002) A47–A50.
[16] P.S. Herle, B. Ellis, N. Coombs, L.F. Nazar, Nat. Mater. 3 (2004) 147–152.
[17] M.M. Doeff, Y. Hu, F. McLarnon, R. Kostecki, Electrochem. Solid-State Lett. 6 (2003) A207.
[18] Y. Wang, Y. Wang, E. Hosono, K. Wang, H. Zhou, Angew. Chem. Int. Ed. 47 (2008) 7461.
[19] B.Q. Zhu, X.H. Li, Y.X. Wang, H.J. Guo, Mater. Chem. Phys. 98 (2006) 373.
[20] L. Wang, G.C. Liang, X.Q. Ou, X.K. Zhi, J.P. Zhang, J.Y. Cui, J. Power Sources 189 (2009) 423.
[21] L. Yuan, Z. Wang, W. Zhang, X. Hu, J. Chen, Y. Huang, J. Goodenough, Energy Environ. Sci. 4 (2011) 269–284.
[22] H. Shin, W. Cho, H. Jang, Electrochim. Acta 52 (2006) 1472–1476.
[23] J.-K. Kim, G. Cheruvally, J.-H. Ahn, J. Solid State Electrochem. 12 (2008) 799–805.
[24] K.S. Park, S.B. Schougaard, J.B. Goodenough, Adv. Mater. 19 (2007) 848–851.
[25] E.M. Bauer, C. Bellitto, M. Pasquali, P.P. Prosini, G. Righini, Electrochem. Solid-State Lett. 7 (2004) A85–A87.
[26] I.V. Thorat, V. Mathur, J.N. Harb, D.R. Wheeler, J. Power Sources 162 (2006) 673–678.
[27] X. Li, F. Kang, X. Bai, W. Shen, Electrochem. Commun. 9 (2007) 663–666.
[28] C.W. Ong, Y.K. Lin, J.S. Chen, J. Electrochem. Soc. 154 (2007) A527–A533.
[29] K.S. Dhindsa, B.P. Mandal, K. Bazzi, M.W. Lin, M. Nazri, G.A. Nazri, V.M. Naik, V.K. Garg, A.C. Oliveira, P. Vaishnava, R. Naik, Z.X. Zhou, Solid State Ionics 253 (2013) 94–100.
[30] J.H. Hong, Y.F. Wang, G. He, M.Z. He, Mater. Chem. Phys. 133 (2012) 573.
[31] K. Zaghib, J. Shim, A. Guerfi, P. Charest, K.A. Striebel, Electrochem. Solid-State Lett. 8 (2005) A207–A210.
[32] S.S. Zhang, J.L. Allen, K. Xua, T.R. Jow, J. Power Sources 147 (2005) 234–240.
[33] Y.D. Cho, G.T.K. Fey, H.M. Kao, J. Power Sources 189 (2009) 256–262.
[34] B. Zhao, Y. Jiang, H. Zhang, H. Tao, M. Zhong, Z. Jiao, J. Power Sources 189 (2009) 462–466.
[35] D. Zhang, X. Yu, Y. Wang, R. Cai, Z. Shao, X.Z. Liao, Z.F. Ma, J. Electrochem. Soc. 156 (2009) A802–A808.
[36] G.T.K. Fey, T.L. Lu, F.Y. Wu, W.H. Li, J. Solid State Electrochem. 12 (2008) 825–833.
[37] H.C. Wong, J.R. Carey, J.S. Chen, Int. J. Electrochem. Sci. 5 (2010) 1090–1102.
[38] K. Kim, J.H. Jeong, I.J. Kim, H.S. Kim, J. Power Sources 167 (2007) 524–528.
[39] Y.H. Rho, L.F. Nazar, L. Perry, D. Ryan, J. Electrochem. Soc. 154 (2007) A283–A289.
[40] F.Z. Wei, G.X. Feng, L.L. Ping, L.G. Sheb, Z. Jing, Chin. J. Struct. Chem. 30 (2011) 7.
[41] M.T. Paques-Ledent, P. Tarte, Spectrochim. Acta 30 (1974) A673.
[42] K. Bazzi, K.S. Dhindsa, A. Dixit, M.B. Sahana, C. Sudakar, M. Nazri, Z.X. Zhou, P. Vaishnava, V.M. Naik, R. Naik, J. Mater. Res. 27 (2012) 7.
[43] K. Dokko, Q. Shi, I.C. Stefan, D.A. Scherson, J. Phys. Chem. B 107 (2003) 12549–12554.
[44] C. Delmas, H. Cognac-Auradou, J.M. Cocciantelli, M. Ménétrier, J.P. Doumerc, Solid State Ionics 69 (1994) 257–264.
[45] M. Guilmard, C. Pouillerie, L. Croguennec, C. Delmas, Solid State Ionics 160 (2003) 39–50.
[46] N.J. Dudney, Electrochem. Soc. Interface 17 (2008) 44–48.
[47] C.H. Mi, X.G. Zhang, X.B. Zhao, H.L. Li, Mater. Sci. Eng. B Solid State Mater. Adv. Technol. 8 (2006) 12.
[48] C.M. Burba, R. Frech, J. Electrochem. Soc. 151 (2004) A1032.
[49] U.J. Kim, C.A. Furtado, G.C.X. Liu, P.C. Eklund, J. Am. Chem. Soc. 127 (2005) 15437.
[50] K. McGuirea, N. Gothard, P.L. Gai, M.S. Dresselhaus, G. Sumanasekera, A.M. Rao, Carbon 43 (2005) 219.
[51] K. Zaghib, A. Mauger, F. Gendron, C.M. Julien, Solid State Ionics 179 (2008) 16.
[52] C.D. Wagner, W.M. Riggs, L.D. Davis, J.F. Moulder, G.E. Mullenberg, Handbook of X-ray Photoelectron Spectroscopy, Perkin-Elmer Corp., Eden Praine, MN, USA, 1979.
[53] A. Yamada, S.C. Chung, K. Hinokuma, J. Electrochem. Soc. 3 (2001) A224.
[54] A.A.M. Prince, S. Mylswamy, T.S. Chan, R.S. Liu, B. Hannoyer, M. Jean, C.H. Shen, S.M. Huang, J.F. Lee, G.X. Wang, Solid State Commun. 132 (2004) 455.
[55] J. Wang, X. Sun, Energy Environ. Sci. 5 (2012) 5163–5185.
[56] D.Y.W. Yu, C. Fietzek, W. Weydanz, J. Electrochem. Soc. 154 (2007) A253–A257.
[57] A. Kumar, R. Thomas, N.K. Karan, J.J. Saavedra-Arias, M.K. Singh, S.B. Majumder, M.S. Tomar, R.S. Katiyar, J. Nanotechnol. 1155 (2009) 176517.
[58] Y. Liu, C. Cao, J. Li, Electrochim. Acta 55 (2010) 3921–3926.
[59] C.M. Doherty, R.A. Carusoab, C.J. Drummondac, Energy Environ. Sci. 3 (2010) 813–823.